Enhanced understanding of atmospheric blocking modulation on ozone dynamics within a high-resolution Earth system model

Wenbin Kou[1], Yang Gao[1]*, Dan Tong[2], Xiaojie Guo[3,4], Xiadong An[5], Wenyu Liu[2], Mengshi Cui[2], Xiuwen Guo[1], Shaoqing Zhang[6], Huiwang Gao[1], Lixin Wu[6]

[1]Frontiers Science Center for Deep Ocean Multispheres and Earth System and Key Laboratory of Marine Environmental Science and Ecology, Ministry of Education, Ocean University of China, and Laoshan Laboratory, Qingdao, 266100, China

[2]Department of Earth System Science, Tsinghua University, Beijing, 100084, China

[3]International Center for Climate and Environment Sciences, Institute of Atmospheric Physics, Chinese Academy of Sciences, Beijing, 100029, China

[4]University of Chinese Academy of Sciences, Beijing, 100049, China

[5]College of Oceanic and Atmospheric Sciences, Ocean University of China, Qingdao, 266100, China

[6]Frontiers Science Center for Deep Ocean Multispheres and Earth System, and Key Laboratory of Physical Oceanography, Ministry of Education, the College of Oceanic and Atmospheric Sciences, Ocean University of China, and Laoshan Laboratory, Qingdao, 266100, China

*Correspondence to: yanggao@ouc.edu.cn

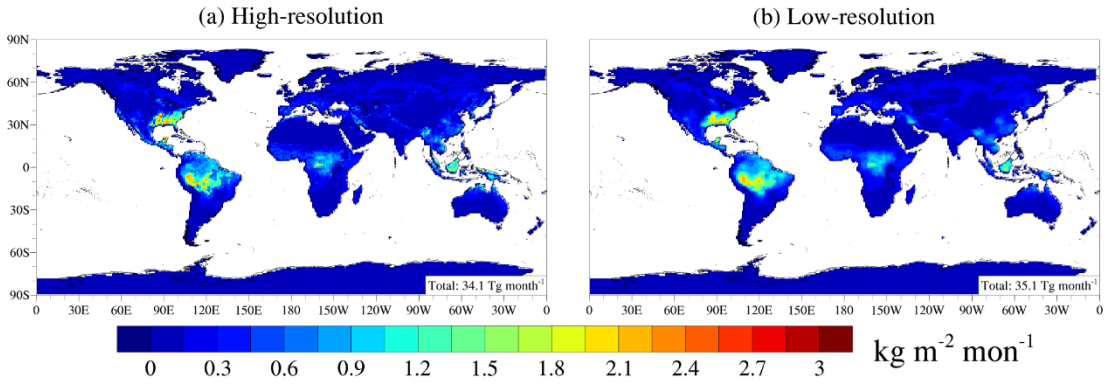

Fig. S1 Spatial distribution of isoprene emissions. Shown are results at high-resolution (0.25°×0.325°) and low-resolution (2°×2.5°) simulations based on Weng et al. (2020).

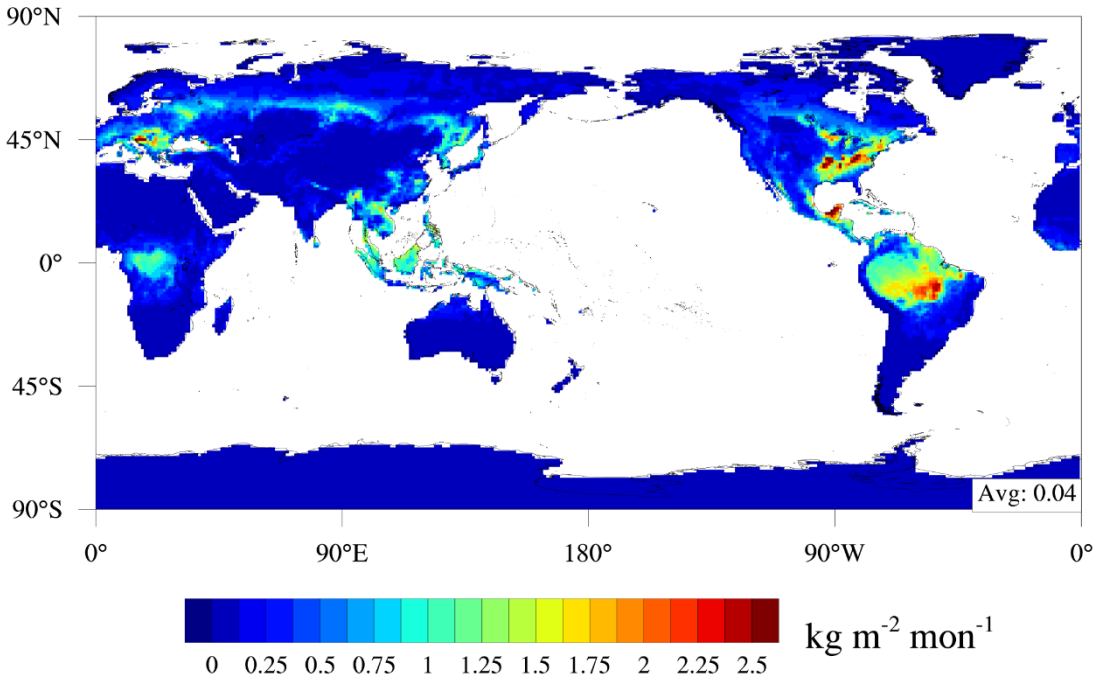

Fig. S2 Spatial distribution of isoprene emission standard deviation in the high-resolution simulations. Shown are results equivalent to the low-resolution grids, with each value representing the standard deviation calculated using the proximately sixteen grids in high-resolution (i.e., 25 km) simulations corresponding to the low-resolution (i.e., 100 km) grid.

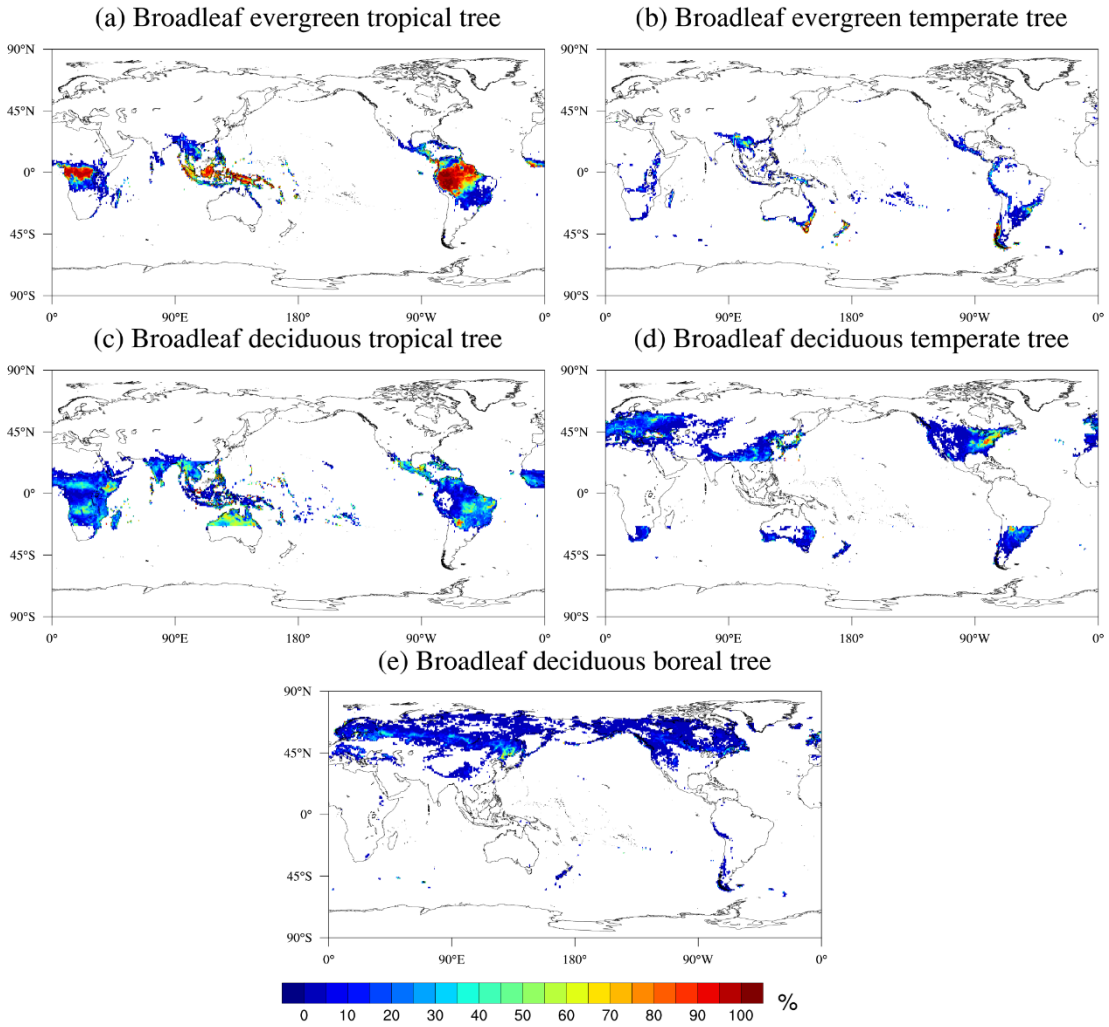

Fig. S3 Spatial distribution of broadleaf trees (%) based on the plant type functions used in global models.

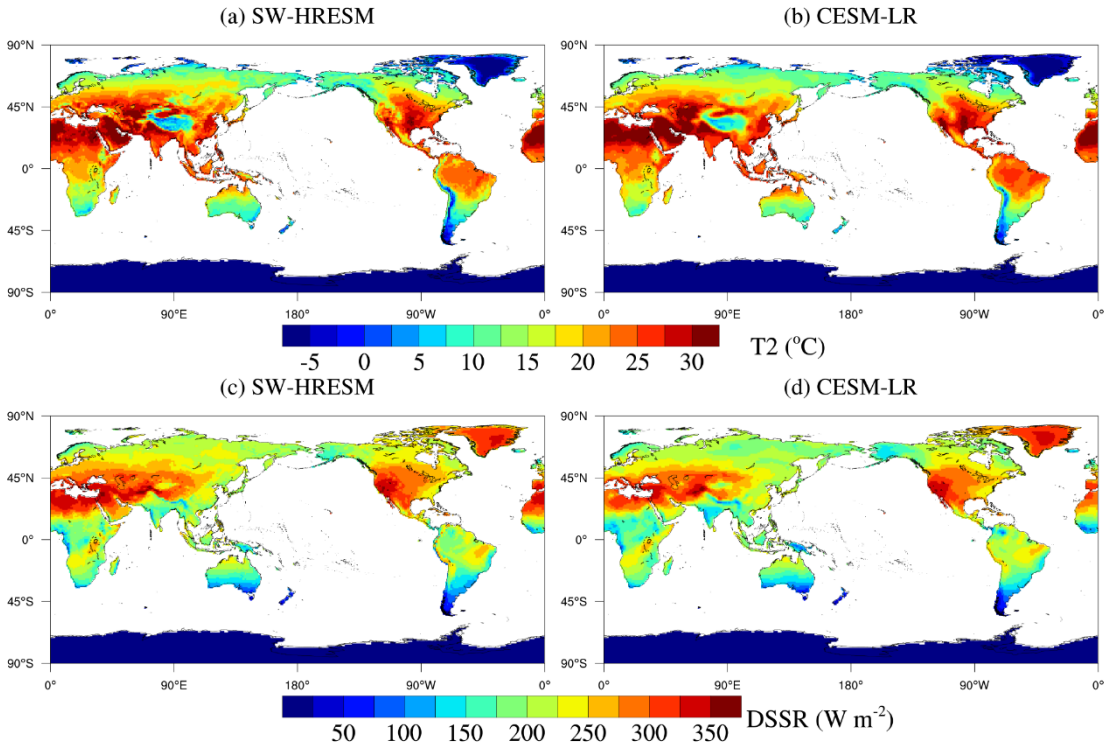

Fig. S4 Spatial distribution of 2-m air temperature and downward surface solar radiation. Shown are results based on SW-HRESM and CESM-LR simulations during the summer of 2015-2019

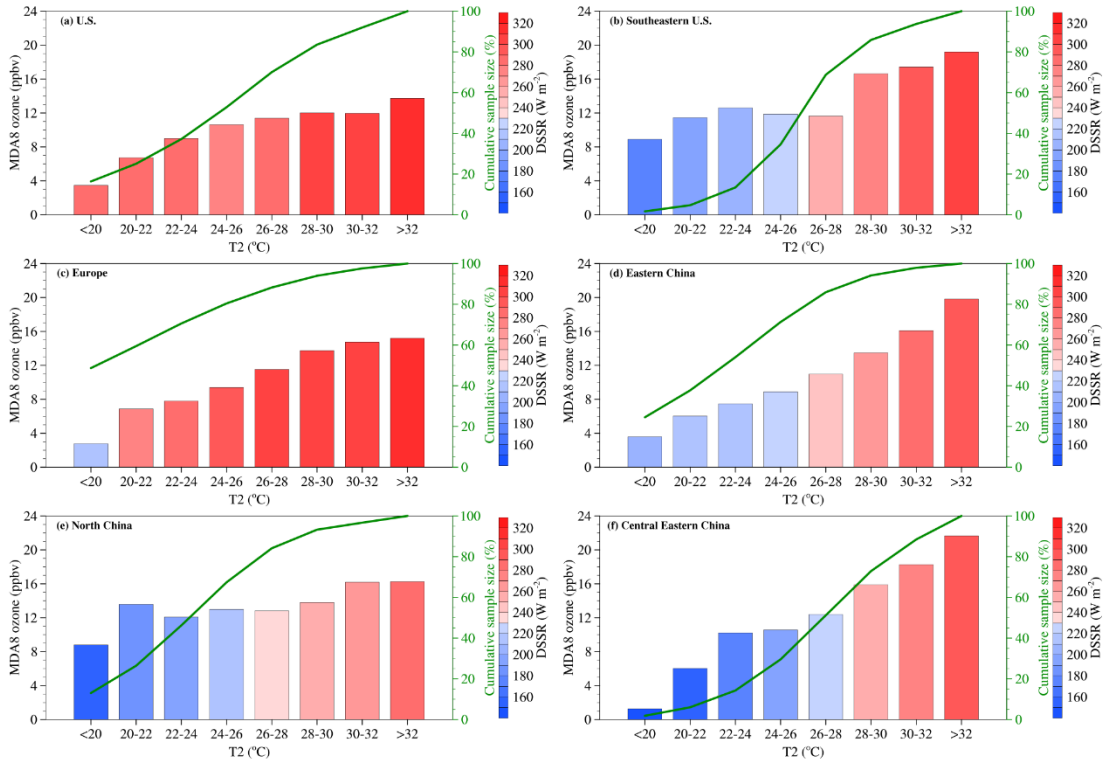

Fig. S5 The contribution of biogenic volatile organic compound emissions to ozone. Shown are results along 2-m air temperature, with shaded color representing downward surface solar radiation (DSSR) over six regions during the summers of 2015-2019. The cumulative sample size over temperature bins is shown in the solid green line.

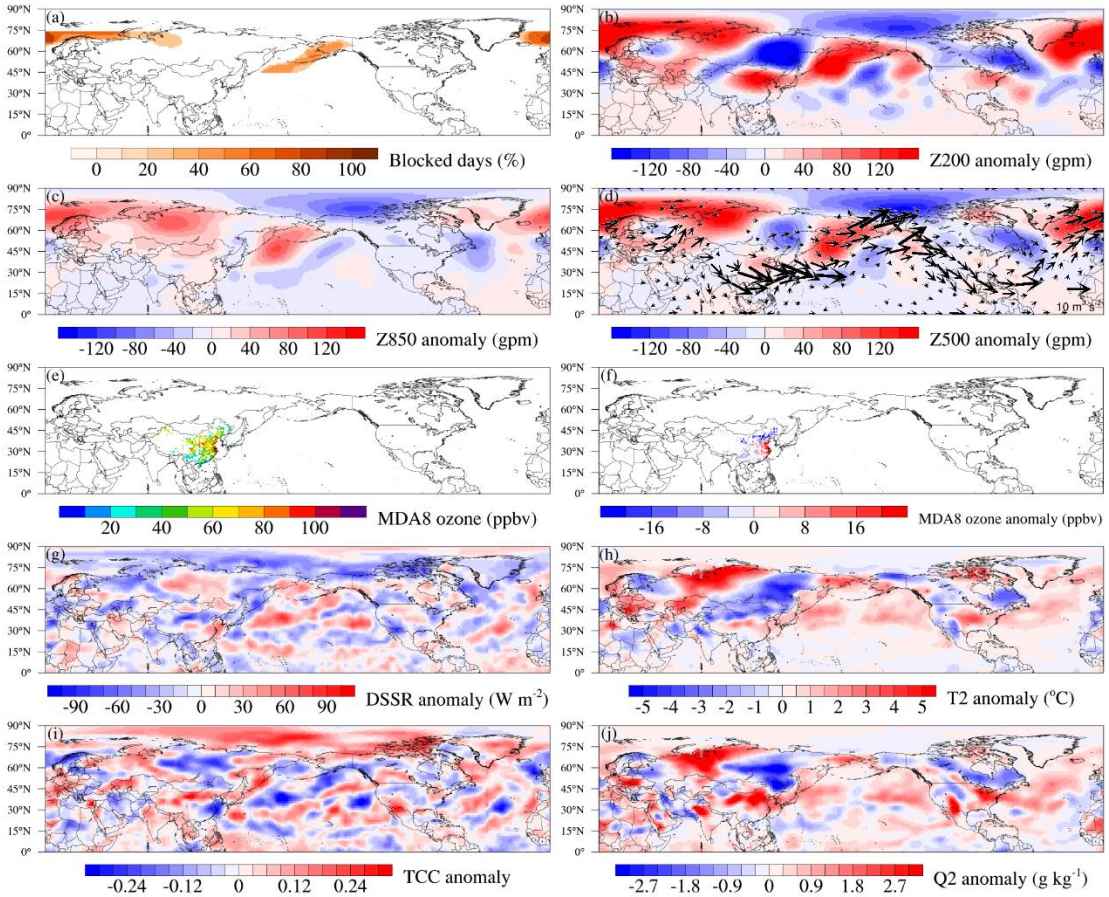

Fig. S6 Spatial distribution of blocking, ozone and geopotential height. Shown are results of anomalies of geopotential height at (b), 200 hPa, (c) 850 hPa, (d) 500 hPa, (e) ozone concentrations, anomalies of (f) ozone, (g), DSSR, (h) 2-m air temperature, (i) total cloud cover and (j) 2-m specific humidity. The results are composited during a specific blocking event over Euro-Atlantic region.

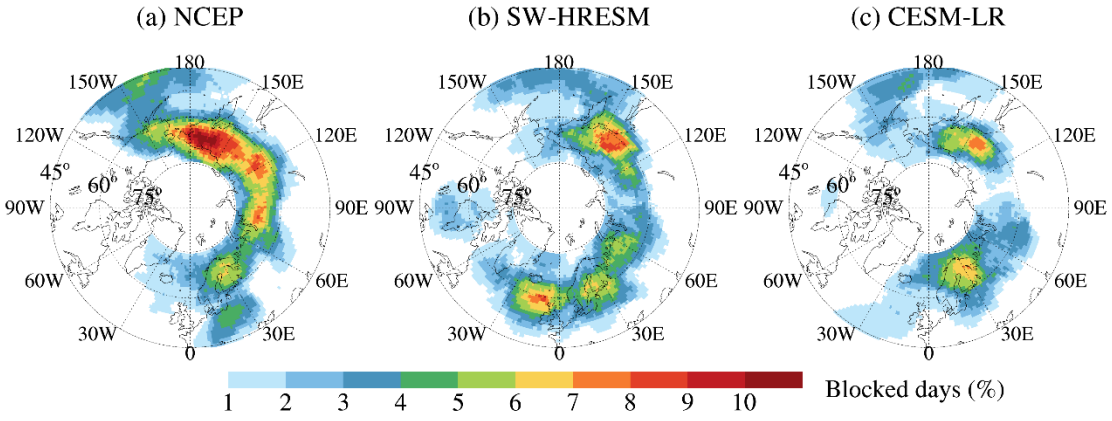

Fig. S7 Mean ratio of atmospheric blocking days based on SW-HRESM and CESM-LR simulations and NCEP reanalysis data during the summer of 2015-2019.

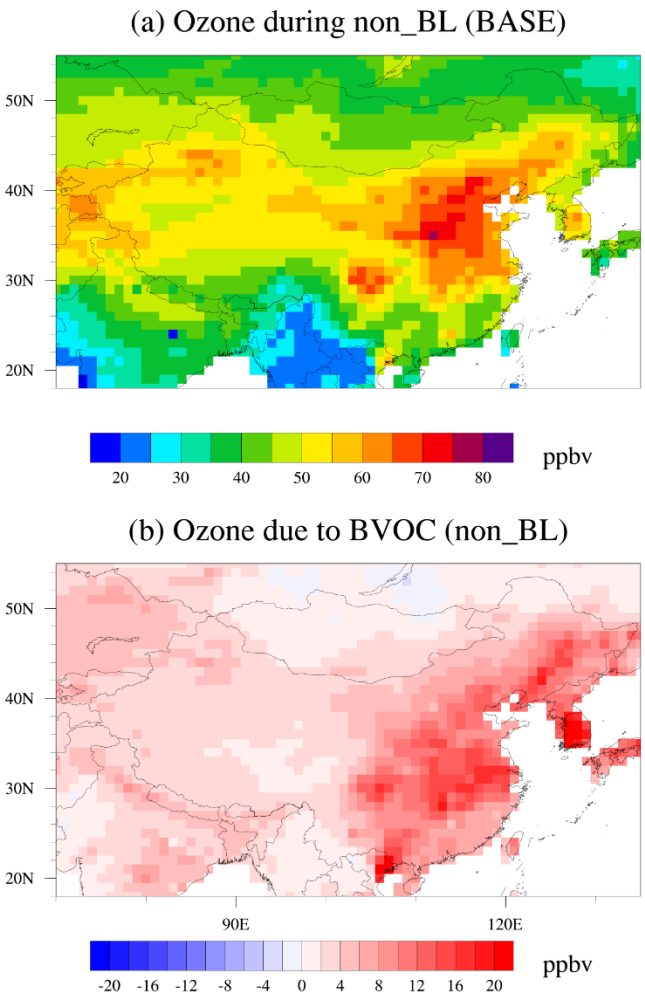

Fig. S8 Spatial distributions of ozone concentrations. Shown are results during non-blocking for (a) BASE and (b) effect of BVOC emissions.

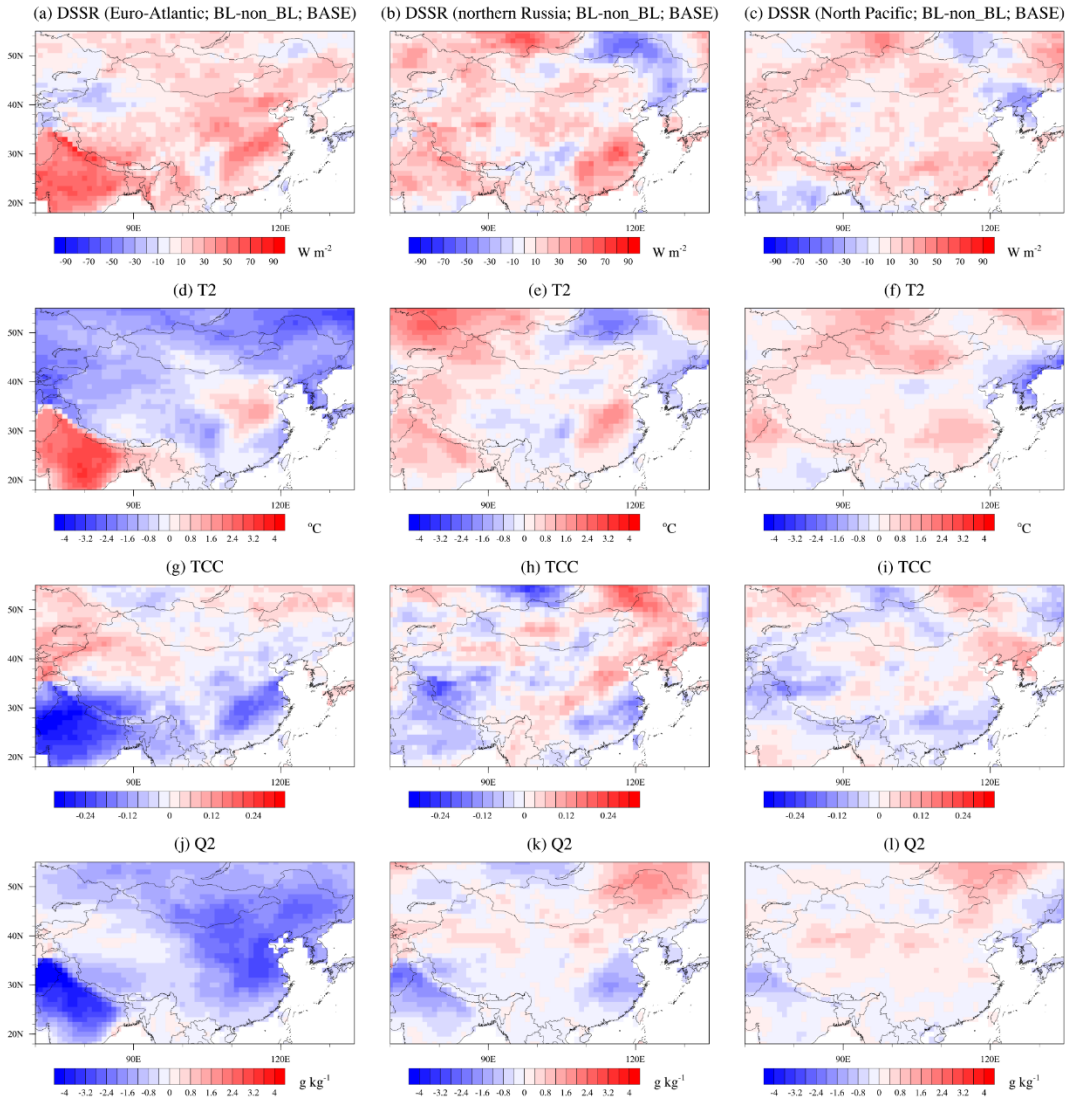

Fig. S9 Spatial distribution of meteorological conditions. Shown are the differences in DSSR (top row), 2-m air temperature (second row), total cloud cover (third row) and 2-m specific humidity (bottom row) during blocking events over Euro-Atlantic (left column), northern Russia (middle column) and the North Pacific (right column) compared to non-blocking periods.

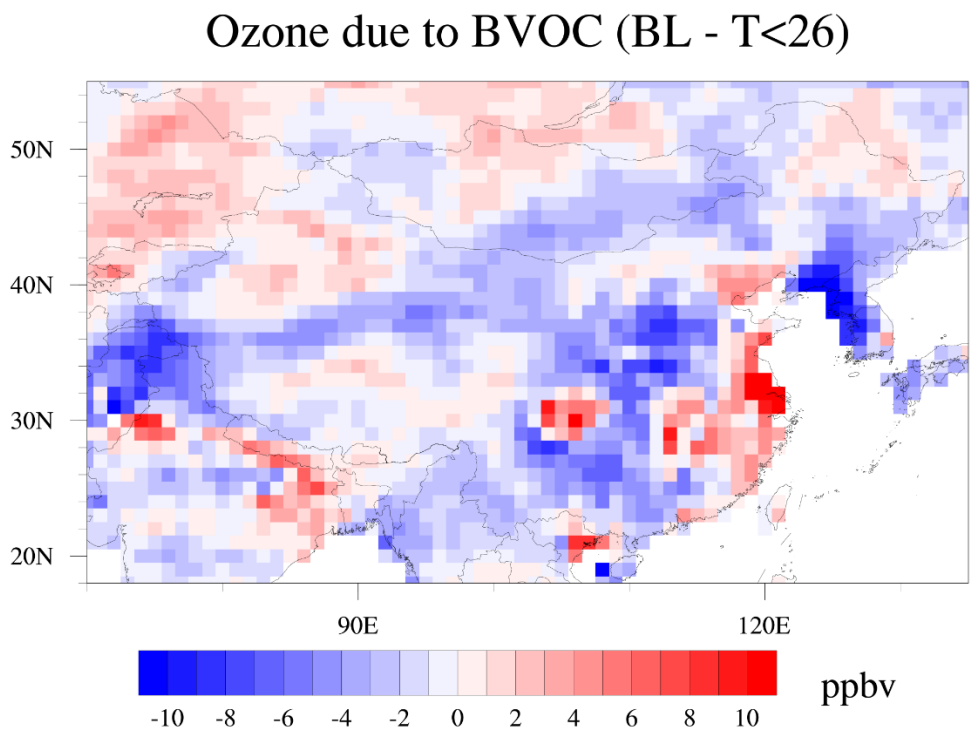

Fig. S10 Spatial distributions of ozone concentrations. Shown are results of the differences in the effects of BVOC emissions on ozone during blocking events over northern Russia, compared to periods with 2-m air temperature below 26 ˚C.